Geophysical Research Letters

RESEARCH LETTER
10.1029/2024GL112387

El Niño Enhances Exposure to Humid Heat Extremes With Regionally Varying Impacts During Eastern Versus Central Pacific Events

Zachary M. Menzo[1], Christina Karamperidou[1], Qinqin Kong[2,3], and Matthew Huber[2]

[1]Department of Atmospheric Sciences, University of Hawai'i at Mānoa, Honolulu, HI, USA, [2]Earth, Atmospheric, and Planetary Sciences Department, The Institute for a Sustainable Future, Purdue University, West Lafayette, IN, USA, [3]Woods Institute for the Environment, Stanford University, Stanford, CA, USA

Abstract Humid heat extremes, characterized by high wet bulb temperature (Tw), pose significant health risks. While strong El Niño events are known to affect the frequency of extreme Tw days, the distinct impacts of Central Pacific (CP) and Eastern Pacific (EP) El Niño events remain understudied. Using a 12-member CMIP6 ensemble at discrete global warming targets (+1.5, 2, 3, 4°C), this study shows progressively enhanced humid heat extent during EP events primarily in Mainland Southeast Asia, while South Asia experiences regionally opposing effects from EP and CP events. EP and CP events drive distinctly different, regionally varying patterns of dangerous Tw, yet both significantly increase the affected population and area impacted by humid heat extremes at all global warming levels. This amplification surpasses the impact of an additional degree of global warming, highlighting El Niño's compounding effect on heat stress threats across warmer climates.

Plain Language Summary Humid heat extremes, characterized by high wet bulb temperature (Tw), pose health risks even to young, healthy individuals. While strong El Niño events are known to affect extreme Tw days, the impact of different El Niño types (Central Pacific and Eastern Pacific) has not been well studied. Using historical data and future climate projections, we examined how these El Niño types affect the frequency and spatial extent of dangerous Tw. Our analysis shows that under future warming, Eastern Pacific and Central Pacific El Niño events drive distinctly different, regionally varying patterns of dangerous Tw, yet both significantly increase the affected population and area impacted by humid heat extremes at all global warming levels. Even at low global warming levels, during El Niño events, the population exposed to dangerous Tw is expected to be equal to that exposed regularly when the mean warming is more than four times higher. This highlights the need to consider El Niño diversity in assessing the additional heat stress in heavily populated regions as the planet warms and approaches the critical threshold of heat stress.

Key Points:

- El Niño events enhance humid heat stress metric exceedances regionally to levels expected under much warmer mean climatological conditions
- Central Pacific events broadly exacerbate humid heat; Eastern Pacific events have localized amplifications but also mitigating effects
- Under future warming, Eastern (Central) Pacific events primarily affect Mainland Southeast (East) Asia; South Asia may see varied effects

Supporting Information:

Supporting Information may be found in the online version of this article.

Correspondence to:

C. Karamperidou,
ckaramp@hawaii.edu

Citation:

Menzo, Z. M., Karamperidou, C., Kong, Q., & Huber, M. (2025). El Niño enhances exposure to humid heat extremes with regionally varying impacts during Eastern versus Central Pacific events. *Geophysical Research Letters*, *52*, e2024GL112387. https://doi.org/10.1029/2024GL112387

Received 17 SEP 2024
Accepted 30 JAN 2025

Author Contributions:

Conceptualization: Zachary M. Menzo, Christina Karamperidou
Data curation: Qinqin Kong, Matthew Huber
Formal analysis: Zachary M. Menzo, Christina Karamperidou
Funding acquisition: Christina Karamperidou
Methodology: Zachary M. Menzo, Christina Karamperidou
Project administration: Christina Karamperidou
Supervision: Christina Karamperidou
Validation: Zachary M. Menzo, Christina Karamperidou

1. Introduction

Heat-related fatalities are a leading cause of death during extreme weather events worldwide (Barriopedro et al., 2011; Buzan & Huber, 2020; Buzan et al., 2015). Elevated environmental humidity further exacerbates heat stress by diminishing the effectiveness of evaporative cooling, the primary mechanism through which humans regulate their internal body temperature (Buzan & Huber, 2020; Coffel et al., 2018; Foster et al., 2021; Im et al., 2017; Raymond et al., 2020; Schär, 2016; Sherwood & Huber, 2010). Humid heat extremes are characterized by high wet bulb temperature (Tw), a measure of the moist enthalpy of the atmosphere (Song et al., 2022). Until recently, most studies used a critical Tw threshold of 35°C which was proposed as the theoretical upper bound of human thermal tolerance, above which the human body cannot dissipate metabolic heat through sensible or latent cooling (Sherwood & Huber, 2010). However, recent findings indicate a lower threshold, dependent on local temperature and humidity conditions, as being more accurate (Vanos et al., 2023; Vecellio et al., 2022, 2024). In high-humidity environments, such as the tropics, exposure to a Tw of 30.6°C for 6 hr poses risks of hyperthermia, heat stroke, or death, even for young, healthy individuals performing minimal metabolic workloads under ideal conditions, that is, full shade, drinking water, minimal exertion (Vecellio et al., 2022). Both the mean moist enthalpy and humid heat extremes are projected to increase in the tropics, spatially coinciding with the fastest projected population growth, underscoring the importance of understanding exposure to Tw (Matthews, 2018).

Visualization: Zachary M. Menzo, Christina Karamperidou
Writing – original draft: Zachary M. Menzo
Writing – review & editing: Zachary M. Menzo, Christina Karamperidou, Qinqin Kong, Matthew Huber

Superposed on the warming trends, natural climate variability in the tropics, dominated by the El Niño Southern Oscillation (ENSO) phenomenon, modulates Tw extremes. Previous studies focused on ENSO impacts on Tw under current climate conditions and found that extreme Tw days are twice as likely during very strong El Niño years compared to neutral years and thrice as likely compared to La Niña years worldwide (Speizer et al., 2022) with the most intense El Niño events resulting in the largest annual average land area affected by extreme Tw days (Rogers et al., 2021). However, the so-called ENSO diversity (Capotondi et al., 2020), that is, the different patterns of SST anomalies during El Niño events whereby the peak SST anomalies are either concentrated in the Eastern Pacific (EP) or Central Pacific (CP) have distinct impacts on extreme events (McKenna & Karamperidou, 2023) and the climate worldwide (Ashok et al., 2007; Capotondi et al., 2020). In this study, we evaluate the escalating impact of the additional heat load imposed by El Niño flavors (EP vs. CP events) in the tropics as the planet approaches the critical threshold of heat stress under discrete global warming targets (GWT) (+1.5, 2, 3, 4°C) using the CMIP6 Tw data set published by Vecellio et al. (2023). We thus address two significant gaps in the literature of Tw extremes in a changing climate: we quantify the superposed impact of El Niño variability on the global warming trend, and we distinguish between the two El Niño flavors, showing the significance of considering their distinct impacts for regional Tw extremes.

2. Data and Methods

2.1. Data

To compute the impact of El Niño flavors on Tw extremes under future climate change scenarios, we use the Tw data set published in Vecellio et al. (2023), who used 2 m temperature, specific humidity, and surface pressure from 12 CMIP6 coupled general circulation models (GCMs) at 3-hourly resolution to calculate Tw under future discrete GWT using the Davies-Jones adiabat Tw approach (Davies-Jones, 2008).

The calculated Tw values were further bias-corrected following a "pseudo-global warming" approach. First, Tw was calculated for both the ERA5 reanalysis (Hersbach et al., 2023) and each CMIP6 model in the baseline period (1950–1976) that precedes the acceleration of global warming. CMIP6 Tw was also calculated for target years representing 1.5, 2, 3, and 4°C of global warming under the Shared Socioeconomic Pathway (SSP)585 scenario. The SSP585 scenario was chosen to maximize available warming targets, and the warming level-oriented approach makes the results robust to the choice of emission scenarios (Seneviratne & Hauser, 2020; Seneviratne et al., 2016). Then, the differences in 3-hourly Tw between the average year of the baseline period and that of years representing a certain warming target were computed for each CMIP6 model and bilinearly interpolated to the ERA5 horizontal grid. The CMIP6-simulated temporal changes in Tw were finally added to the ERA5 Tw for each year within the baseline, providing bias-corrected estimates of Tw under each GWT.

This approach captures seasonal and diurnal variations in Tw changes with global warming, considering potential changes in background circulation attributed to anthropogenic warming. It preserves climate change signals from CMIP6 models while correcting biases in baseline climate state and provides adequate resolution for capturing geographic features and physical processes important for accurate Tw calculations (Freychet et al., 2022; Im et al., 2017; Vecellio et al., 2023). However, the pseudo-global warming approach imposes background warming on historical extreme Tw patterns during El Niño years (Figure S1 in Supporting Information S1), and thus it does not account for changes in El Niño teleconnections, which would alter the response of Tw extremes to El Niño events, or changes in El Niño diversity itself due to global warming. The implications of this methodological approach for interpreting the results are further addressed in Section 4.

2.2. El Niño Diversity Indices

To characterize EP and CP El Niño years, we use the E and C indices proposed by Takahashi et al. (2011). An El Niño year spans from June (Year 0) to May of the following year (Year +1), and EP and CP events are defined when the DJF E and C indices exceed one standard deviation, respectively (Figure S2 in Supporting Information S1). During the period 1950–1976 used in Section 3, we consider 4 EP events (1951, 1957, 1965, 1972) and 3 CP events (1958, 1963, 1968) which agrees with the consensus in prior studies (e.g., Capotondi et al., 2020; McKenna & Karamperidou, 2023). During the selected EP and CP events, the average June–May global mean temperature anomaly is 0.07 and 0.09°C, respectively. Therefore, the events do not contribute to an average global warming that exceeds any of the GWTs considered for our future scenario analysis.

2.3. Humid Heat Metric Calculations

For the projected impacts of El Niño diversity (Section 3), we calculate the number of *dangerous Tw (dTw) days* as the number of days at each grid cell in which the daily maximum Tw exceeds a threshold of 31°C. The departure from the number of days above the threshold under climatological conditions is used to quantify the projected El Niño impact and is hereafter referred to as *anomalous dTw days*. On a day when the temperature reaches this threshold, an individual would face prolonged exposure to hazardous Tw values, posing a severe threat to their health and contributing to the loss of a working day (Buzan & Huber, 2020), impacting the region socially and economically. Significance testing was conducted using a "bootstrapped" 1,000-member ensemble of EP and CP El Niño composites comprised of random samples of equal size to the ones tested (4 and 3 years, respectively), selected with replacement from every GCM ensemble member under each GWT. Differences in dTw compared to climatology were considered significant if they fell above (below) the 90th (10th) percentile of the difference values calculated from the 1,000-member ensemble for more than half of the models (Figure S3 in Supporting Information S1).

To assess whether the duration of dangerous Tw conditions during EP and CP years changes in the future, we compute the maximum number of consecutive (MC) days exceeding the 31°C threshold. To estimate changes in the spatial extent of the impacts, we calculate the total land area in square kilometers in five regions (West Africa, the Middle East, South Asia, East Asia, and Mainland Southeast Asia) and, for each region, the total land area experiencing dTw for at least 1 day during each El Niño year (Section 3.2). We conduct an independent *t*-test across all models and El Niño events for each region to assess the statistical significance of differences in the total land area affected. To determine the population affected by dTw for at least 1 day during every El Niño year for each GWT, we use the population projections from the SSP2 scenario for the same five regions (Jones & O'Neill, 2016). SSP2 is a "middle-of-the-road" scenario and is considered the most-likely pathway. It assumes medium mortality, fertility, and migration at the country level and is compatible with all GWTs considered. Since the global population under SSP2 is projected to stabilize around 2040, we use the 2050 SSP2 population for all GWTs, consistent with Vecellio et al. (2023). This approach avoids additional complexities from population changes when quantifying the relative impact of El Niño events and additional global warming, which is the focus of this study, and is robust to the choice of population levels (cf. Figure 3; Figure S8 in Supporting Information S1).

3. Impacts of El Niño Diversity on Tw in Warmer Climates

3.1. Dangerous Tw Days

Under future GWT conditions, we find that EP and CP El Niño events impact the frequency, duration, and spatial extent of dTw days in five regions: West Africa, the Middle East, South Asia, East Asia, and Mainland Southeast Asia (Figure 1; see Figure S4 in Supporting Information S1 for a global map and S5 for the relative change in the number of dTw days from one GWT to the next). In all regions, few to no days exceed the 31°C threshold under climatological or El Niño conditions for the first two GWTs (1.5, 2°C). However, consistent with findings by Vecellio et al. (2023), the number of dTw days increases substantially under climatological conditions for the latter two GWTs (3, 4°C), while our analysis additionally reveals that the role of El Niño in modulating the heat stress also becomes significant under these high GWTs.

In the Middle East, Mainland Southeast Asia, and to a lesser extent East Asia, the climatological conditions result in few dTw days, even at a 4°C GWT. However, at the lower GWT of 3°C, El Niño events lead to a substantial increase in dTw days, underscoring El Niño's significant role in exceeding the critical physiological threshold. A similar yet weaker signal is found in the MC days exceeding the threshold, detailed in Supporting Information S1 (Figures S6 and S7).

El Niño has the weakest impact in West Africa (Figure 1a), where a marginal increase is found for both flavors, adding approximately 8–12 dTw days to the weak climatological signal under a 4°C GWT. The change in MC days above the threshold follows similar patterns and increases by about 2–4 days (Figure S7a in Supporting Information S1). CP events primarily impact the northern portions of central Africa, increasing the MC days by up to a week.

The primary impact of El Niño on dTw occurs in South Asia (Figure 1b). Under a GWT of 4°C, the entire Ganges River and Indus Valley regions experience an average of around 40 dTw days, with a minimum of nearly 30 days

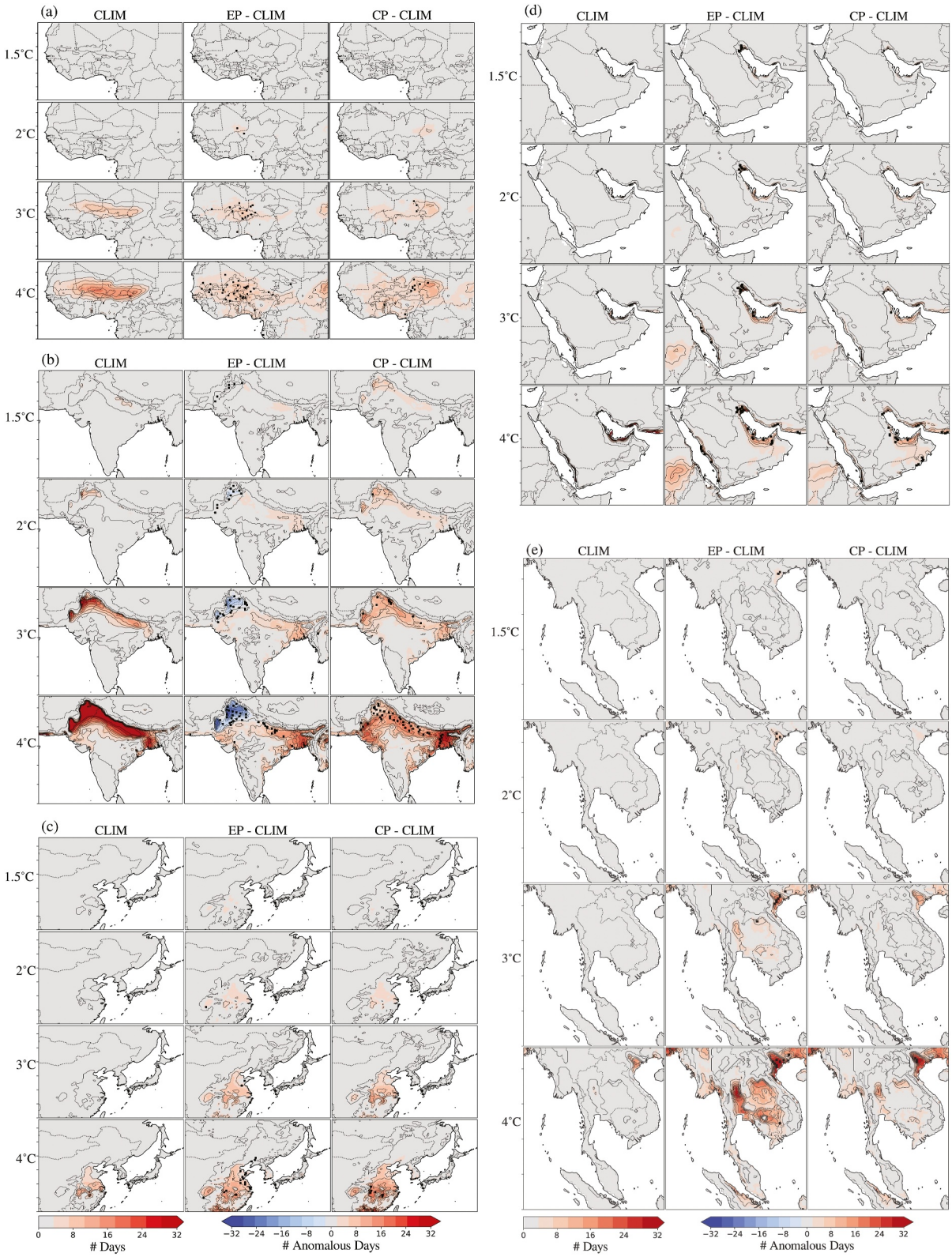

Figure 1. Number of dTw days (daily max Tw > 31°C) per year (June–May) in climatology (CLIM), and the anomalous dTw days in the EP Niño composite (EP—CLIM), and the CP Niño composite (CP—CLIM) under the GWTs (1.5, 2, 3, and 4°C) for (a) West Africa, (b) South Asia, (c) East Asia, (d) the Middle East, and (e) Mainland Southeast Asia. Stippling shows where differences are statistically significant at the 90th percentile for more than half of the models based on a 1,000-member bootstrap ensemble per GCM.

in the former and reaching a maximum of approximately 65 days in the latter. During EP years, the largest increases of dTw days (20–30 days) are found in the Ganges River delta, doubling the climatological signal. In contrast, in the Indus Valley, where the climatology reaches its peak impact, there is a decrease of 20–30 dTw days and nearly a 6–30 days shorter MC streak (Figure S7b in Supporting Information S1). During CP years, much of the Indus Valley and Ganges River regions experience an increase of 12–20 dTw days, while the Ganges River delta and the adjacent region of India have an increase of approximately 25–35 days. This dipole in the impact of the two El Niño flavors can be explained by the strong mitigating effect that EP events have on daily maximum Tw in the Indus Valley region, which does not allow the climatological increase of Tw under the high GWTs to result in exceedance of the 31°C threshold (Figure S1 in Supporting Information S1).

In the Middle East (Figure 1d), the impact of El Niño is confined to the coastlines. The impact is stronger during EP years, with an increase of up to 20 dTw days. CP events show a similar spatial impact but a weaker magnitude, increasing around 12 days, peaking along the southwest. While the impact on the MC days for both El Niño flavors is weak, it does increase the duration by about 2–4 days (Figure S7d in Supporting Information S1).

In East Asia (Figure 1c), under the GWT 4°C scenario, we find the same spatial impact for both El Niño flavors on the number of dTw with greater magnitude during CP years. The impact is evident in Eastern China, with increasing magnitude from north to south. During EP (CP) years, this section of China sees an increase of approximately 6–15 (6–21) dTw days with an increased duration of MC days by about 2–3 (2–6) days (Figure S7c in Supporting Information S1), impacting the region, which has a weak or nonexistent signal under climatological conditions. This pattern reverses to the south in Mainland Southeast Asia (Figure 1e), with EP having a greater spatial increase and impact. During CP years, the northeast region experiences an increase of nearly 20–30 dTw days, with limited sections across the remainder of the peninsula having an increase of up to 15 days. In EP years, the northeast region shows nearly an increase between 25 and 40 dTw days, with most of the peninsula increasing by up to ∼20 days and smaller portions experiencing an increase of around 30 days. During both flavors, the northeast region MC days are about 2–4 days longer (Figure S7e in Supporting Information S1), with other sections of the peninsula showing the same signal during EP years.

3.2. Total Area Affected (%)

The impact of EP and CP events on the percentage of land areas affected by dTw is statistically significant globally and in all high-impact regions across GWTs, excluding West Africa under GWTs of 1.5 and 2°C, compared to the total area affected under climatological conditions (Figure 2). The seasonal variations of this impact shown in Figure 2 could provide valuable insights for regions reliant on outdoor labor or agricultural activities during specific seasons. Globally, the overall impact of both El Niño flavors and their seasonal peak is nearly identical. However, the difference between EP and CP events becomes more pronounced when examining each high-impact region, highlighting the necessity for regional analysis of area affected by dangerous Tw conditions. At a GWT of 4°C, West Africa experiences its peak impact during SON, with 13% more land area being impacted during EP years and 11% during CP years than what would be expected under climatological conditions. EP events have the maximum impact during JJA in South Asia and Mainland Southeast Asia, with 13% and 28% more land area being impacted, respectively. During CP years, the greatest impact is found during the SON season, with approximately 17% more land area being impacted relative to climatological conditions in both regions. However, Mainland Southeast Asia shows very weak seasonality, excluding the DJF season. Finally, in the Middle East and East Asia, the peak impact of both El Niño flavors occurs during the JJA season. In the Middle East (East Asia), 11.5% (13%) more land area is impacted during EP years, while 9% (16%) more land area is impacted during CP years than what would be expected under climatological conditions.

Importantly, under a given GWT, El Niño events create conditions that are similar to or worse than those expected climatologically under warmer mean climate conditions. To show this, we calculate the difference between the anomalous total area affected during EP or CP events at a given GWT $[TA_{ij} - \overline{TA}_j]$ and the additional total area affected under climatological conditions at the next higher GWT $[\overline{TA}_{j+1} - \overline{TA}_j]$ (Equation 1), shown in dashed lines in Figure 2.

$$[TA_{ij} - \overline{TA}_j] - [\overline{TA}_{j+1} - \overline{TA}_j] = TA_{ij} - \overline{TA}_{j+1} \quad (1)$$

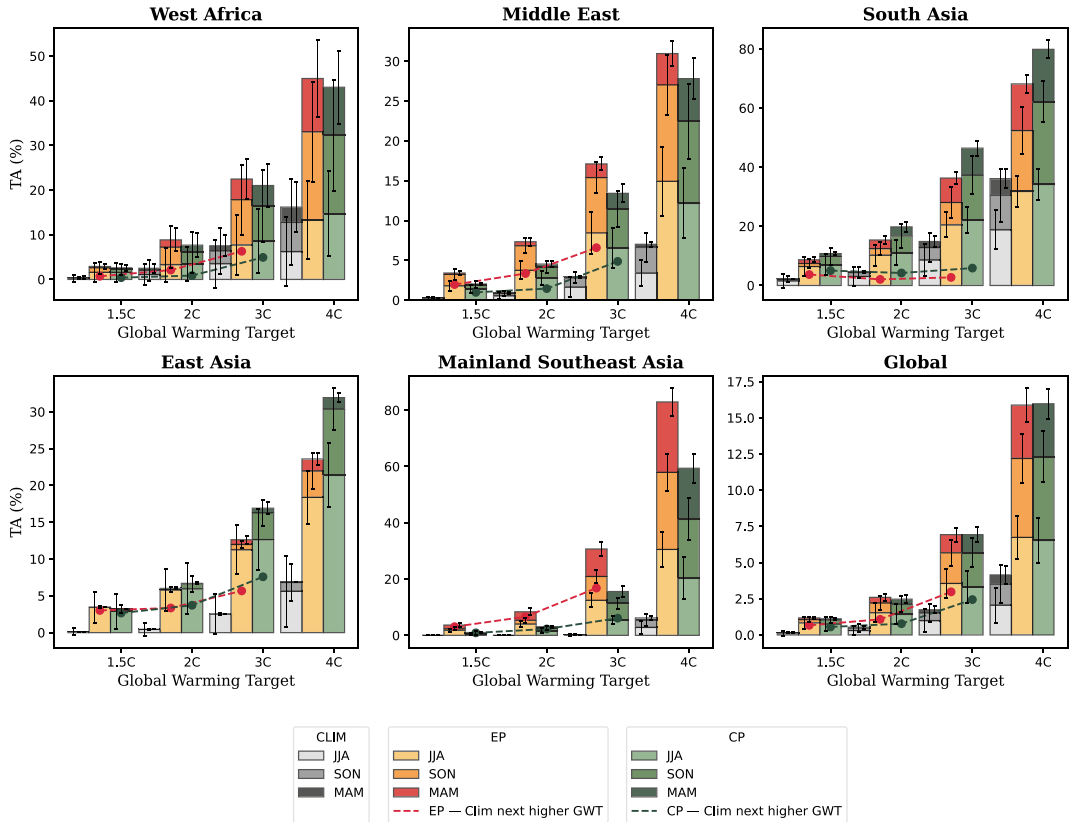

Figure 2. Percentage of total land area experiencing at least 1 day with dTw at each location under the four GWTs. Shades of gray, red, and green represent the seasons during climatological, EP, and CP Niño years, respectively. The lightest (darkest) shade indicates JJA (MAM) season. Seasonal error bars for each El Niño flavor represent one standard deviation determined from the multi-model ensemble. Red (Green) dashed lines represent the annual total difference between EP (CP) Niño years at a given GWT and the climatology under the next higher GWT.

where $i \in \{\mathrm{EP}, \mathrm{CP}\}$, $j \in \{1.5, 2, 3, 4^{\circ}\mathrm{C}\}$, and $\overline{\mathrm{TA}}$ is the total area affected under climatological conditions.

The difference calculated by Equation 1 is positive in all regions and globally, indicating that the spatial impact of El Niño events matches or exceeds the conditions expected on average under the next higher GWT. Furthermore, the relative importance of the El Niño impact compared to background warming, and predominantly that of EP events (red dashed lines), increases with warming, as the value of Equation 1 increases in all regions except South Asia.

In certain regions, El Niño can even have an impact equal to or greater than the climatology at twice the GWT. For example, during EP years in the Middle East and Mainland Southeast Asia, or during both El Niño flavors in East Asia, more land is affected by dangerous Tw conditions under a 1.5°C GWT than during climatology for a 3°C warming scenario.

3.3. Population Exposure to Dangerous Tw

Following the increase in total area experiencing dTw conditions (Figure 2), El Niño events increase the affected population between 1.5 and 32 times in high-impact regions and by 2–6 times globally, compared to climatological conditions across various GWTs (Figure 3). This underscores the importance of adopting a regional perspective to accurately assess the impact in specific locations where the effects can far exceed the global average. Similar to Figure 2, the dashed lines in Figure 3 compare the impact of El Niño on population exposure under a given GWT with the climatological impact of the next higher GWT (Equation 2).

$$\left[\mathrm{PE}_{ij} - \overline{\mathrm{PE}}_{j}\right] - \left[\overline{\mathrm{PE}}_{j+1} - \overline{\mathrm{PE}}_{j}\right] = \mathrm{PE}_{ij} - \overline{\mathrm{PE}}_{j+1} \quad (2)$$

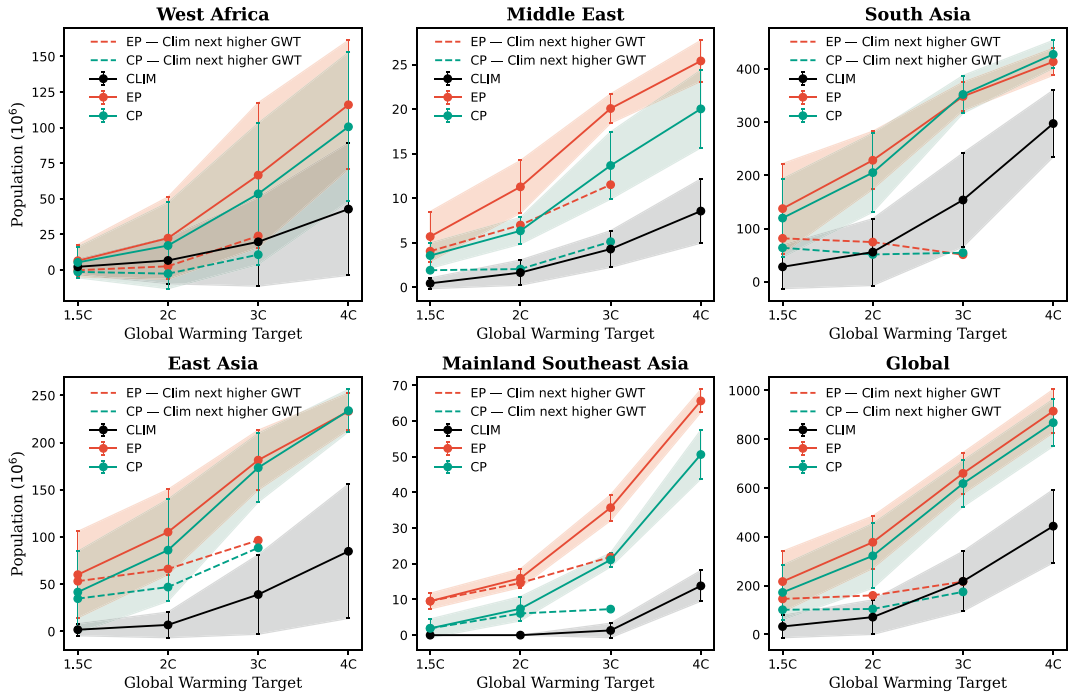

Figure 3. Population (in millions; following 2050 SSP2 population projections) exposed to at least 1 day with dTw per year (daily max Tw > 31°C) at each location under the four GWTs. Black lines represent the climatology, with the red line indicating EP years and the green line representing CP years. Error bars represent one standard deviation determined from the multi-model ensemble. Red (Green) dashed lines represent the difference between EP (CP) Niño years at a given GWT and the climatology under the next higher GWT.

where $i \in \{\mathrm{EP}, \mathrm{CP}\}$, $j \in \{1.5, 2, 3, 4^\circ\mathrm{C}\}$, and $\overline{\mathrm{PE}}$ is the Population Exposure under climatological conditions.

With the exception of West Africa under 1.5 and 2°C GWTs, El Niño leads to a greater population exposure at a given GWT than what is caused climatologically at the next GWT. In the Middle East and East Asia, the relative impact of El Niño increases with background warming, while in Mainland Southeast Asia or South Asia the added impact of El Niño is weakened with higher GWTs, as indicated by the steady or decreasing values of Equation 2 (even though in absolute numbers the affected population will be larger). In regions where the population climatologically exposed to at least one dTw day is near zero for the lower GWTs (e.g., Middle East and East Asia for GWT of 1.5°C, and Mainland Southeast Asia for GWT of 1.5, 2, and 3°C), as well as on a global scale at a 1.5°C GWT, El Niño events increase the population exposure to levels expected under climatological conditions for the highest GWTs (3 or 4°C). In general, EP El Niño events have stronger impacts compared to CP events, however, these are only well separated statistically in the Middle East and Mainland Southeast Asia.

In South Asia, East Asia, and the Middle East, the impact of El Niño under a 1.5°C warming scenario exceeds that of a 2°C GWT during climatology by a factor of 2–9. Similarly, under a 2°C (3°C) warming scenario, the impact is 1.5–3 (1.2–2.3) times greater compared to climatology under a 3°C (4°C) GWT. While the impact of El Niño events remains high under the 4°C GWT, the population exposed to at least one dTw day per year under climatological conditions grows at a similar or faster rate. In other words, under higher GWTs, the population is already routinely affected by dTw (i.e., climatologically), which diminishes the added impact of El Niño. Nonetheless, in terms of the number of people affected and in terms of additional heat stress (leading to Tw values well above the 31°C threshold), El Niño events remain highly consequential in these densely populated regions regardless of the population scenario (Figure 3; Figure S8 in Supporting Information S1). In the Middle East, EP events have a significantly stronger impact compared to CP events, while in South and East Asia, EP events exhibit a slightly greater impact than CP under lower GWTs, but the difference is minimal and not statistically significant, with any distinction between flavors diminished at higher GWTs. The similarity in population exposure during EP and CP events in South Asia may seem surprising since CP events have a larger impact on total dTw compared to EP events (Figure 1b). However, in the SSP2 2050 population projections (Figure S9 in

Supporting Information S1), most of the population lives near the Ganges River delta. Under the lower GWTs (1.5 and 2°C), the impact of EP events better aligns with the most populous locations, while under the latter two GWTs (3 and 4°C), the impact of CP events spreads to these areas, matching and surpassing the impact of EP events, possibly explaining the lack of statistical difference between El Niño flavors. In the Middle East, EP events remain dominant under all GWT, having a 1.5–2 times greater impact than CP events, underscoring the significance of distinguishing between El Niño flavors for this region.

In West Africa, the number of people exposed to at least one dTw day per year increases by a factor of 2.5–4 during El Niño years compared to climatology across all GWTs, with EP having 1.2 times the impact compared to CP years under higher GWT.

In Mainland Southeast Asia, El Niño events have a profound impact, increasing the projected total population exposure to dTw in a region that would not have significantly surpassed that threshold under climatological conditions until a 4°C GWT. For example, the population impacted during EP (CP) events under a 1.5°C (2°C) GWT approaches values observed under a 4°C GWT during climatology, while the impact of EP (CP) events under a 2°C warming scenario exceeds that of a 3°C GWT during climatology by a factor of 12 (6). The impact of both El Niño flavors grows exponentially with higher GWT, with EP events being dominant across all warming scenarios, at least doubling the affected population compared to CP events under the lower GWTs. The impacts of EP and CP events are well separated for all GWTs, indicating that skillful predictions of EP versus CP El Niño will continue to be of great significance for anticipating its effects on Tw extremes in this region.

4. Summary and Discussion

This study investigates the distinct impacts of EP and CP El Niño events on dangerous Tw (dTw) under future climate change conditions, using a downscaled 12-member CMIP6 ensemble across various GWT (+1.5, 2, 3, 4°C). Under future GWTs, EP El Niño leads to a greater increase in the frequency of dTw days in Mainland Southeast Asia, whereas CP El Niño leads to a higher number of dTw days in East Asia. In South Asia, EP and CP events have opposing impacts in the Indus Valley, but both increase the number of dTw days in the Ganges River regions, with a more pronounced effect during CP years. Across all locations and GWTs, El Niño events also result in a substantial amplification of population exposure to at least one dTw day per year compared to climatological conditions, with the impacts of EP events being stronger than those of CP events, most robustly in the Middle East and Mainland Southeast Asia. Similarly, El Niño significantly expands the area affected by at least 1 day with dTw per year compared to climatological conditions. EP El Niño has the greatest impact in Mainland Southeast Asia compared to CP events, particularly under GWTs of 3–4°C. In contrast, CP events have a greater impact in South and East Asia at higher GWT, with limited differences in impact in West Africa or the Middle East.

This study highlights the need for integrating El Niño diversity into assessments of Tw extremes and their implications for human health, as different regions can experience varying and sometimes opposing effects during EP and CP El Niño events. The distinct impacts of these events in tropical and extratropical atmospheric circulation arise from differential shifts in tropical convection in response to their respective SST anomaly patterns (Ashok et al., 2007; Capotondi et al., 2015; Lu et al., 2020; McKenna & Karamperidou, 2023). Given that ENSO is a significant source of seasonal climate predictability, improved predictions of El Niño diversity several months in advance (e.g., Rivera Tello et al., 2023) can lead to advanced warnings for improved emergency management in densely populated regions affected by extreme Tw.

It is important to interpret the results of this study within the context of its pseudo-global warming approach for calculating future Tw. While this approach mitigates biases, it does not account for potential changes in El Niño diversity and its teleconnections under warmer climates, which could subsequently alter the Tw pattern response to these events. Even without changes in ENSO itself, changes in the background climate, such as an El Niño- or La Niña-like change in surface temperatures in the tropical Pacific, can impact ENSO teleconnections. For example, Karamperidou (2024) showed that ENSO-scale variability of summertime atmospheric blocking events, which are often associated with prolonged heatwaves, is modulated by the background state of the tropical Pacific. Additionally, changes in the tropical Pacific background state may also alter ENSO variance (Cai et al., 2021; Karamperidou et al., 2017; Wyman et al., 2020) and skewness, that is, the relative frequency of strong El Niño versus strong La Niña events (Liu et al., 2023). These changes could the frequency, pattern, and severity of Tw extremes, as both El Niño and La Niña events shift the regions experiencing hot and humid conditions (e.g.,

Jia et al., 2024). This study focuses exclusively on the warm phase (El Niño) of ENSO and its diversity, and does not address the potential impacts of changes in the tropical Pacific's background state on the response of Tw extremes to El Niño; future investigations will explore these important issues. Given the uncertainties in the response of the relative frequency of EP and CP El Niño events to external forcing (Cai et al., 2021; Capotondi et al., 2020; Karamperidou & DiNezio, 2022) and potential future changes in El Niño flavor teleconnections (Taschetto et al., 2016), as well as the complexities arising from model limitations, internal climate variability, and the different forcings and feedbacks across climate scenarios, we propose that the pseudo-global warming approach's inherent assumption of unchanged El Niño teleconnections is reasonable and allows to isolate the role of El Niño in modulating humid heat extremes across different global warming targets that do not represent a single specific forcing scenario.

Within this context, our analysis of the area impacted by humid heat extremes and subsequent population exposure to dangerous humid heat under various GWTs shows that both EP and CP El Niño events result in impacts that are comparable to or exceed those anticipated climatologically under much warmer background climates. This holds true even for low GWTs (e.g., 1.5°C) in regions where there is minimal to no impact from dTw under climatological conditions. This finding echoes the current practice of often referring to El Niño events and their associated global temperature extremes as potential analogs for the future. The exponential increase in the affected area and population exposure due to dTw during El Niño events at progressively warmer background climates can have significant implications for preparedness. For instance, an EP event at 1.5°C warming that results in a much greater population exposure than what is climatologically expected at the 4°C warming level (e.g., in the Middle East) would necessitate that governments allocate resources that would not typically be considered until 50 or more years into the future. Thus, the widely acknowledged "far-reaching" impacts of El Niño and its diversity not only span different regions but also pull future challenges closer to the present.

Conflict of Interest

The authors declare no conflicts of interest relevant to this study.

Data Availability Statement

ERA5 data and SSP population data are publicly available from the Copernicus Climate Change Service (C3S) Climate Data Store (CDS) (Hersbach et al., 2023) and the earthdata catalog (Jones & O'Neill, 2020), respectively. The Wet-Bulb Temperature algorithm was created by Buzan et al. (2015) and converted to Python by Simpson, Brousse, Ebi, and Heaviside (2023) and Simpson, Brousse, Heaviside, & Ebi (2023). Data sets for this research are available on Zenodo (Menzo et al., 2024). The bias-corrected CMIP6 Tw data set is freely available at Purdue Fortress long-term archive; the metadata, including a data set inventory and access instructions, are deposited on Zenodo (Kong & Huber, 2024).

Acknowledgments
ZM and CK were supported by National Science Foundation Grants AGS-1902970 and AGS-2202663. This work was also partially supported by NSF Grant ERC-2330175 for the Engineering Research Center EARTH. QK and MH were supported by NASA FINESST Grant 80NSSC22K1544; Grant NSF 1805808-CBET Innovations at the Nexus of Food, Energy, and Water Systems (INFEWS: U.S.-China): A multi-scale integrated modeling approach to managing the transition to sustainability; NSF 1829764-OAC CyberTraining: CIU: Cross-disciplinary Training for Findable, Accessible, Interoperable, and Reusable (FAIR) science. This is SOEST contribution #11884.

References

Ashok, K., Behera, S. K., Rao, S. A., Weng, H., & Yamagata, T. (2007). El Niño Modoki and its possible teleconnection. *Journal of Geophysical Research*, *112*(C11), C11007. https://doi.org/10.1029/2006JC003798

Barriopedro, D., Fischer, E. M., Luterbacher, J., Trigo, R. M., & García-Herrera, R. (2011). The hot summer of 2010: Redrawing the temperature record map of Europe. *Science*, *332*(6026), 220–224. https://doi.org/10.1126/science.1201224

Buzan, J. R., & Huber, M. (2020). Moist heat stress on a hotter Earth. *Annual Review of Earth and Planetary Sciences*, *48*(1), 623–655. https://doi.org/10.1146/annurev-earth-053018-060100

Buzan, J. R., Oleson, K., & Huber, M. (2015). Implementation and comparison of a suite of heat stress metrics within the Community Land Model version 4.5. *Geoscientific Model Development*, *8*(2), 151–170. https://doi.org/10.5194/gmd-8-151-2015

Cai, W., Santoso, A., Collins, M., Dewitte, B., Karamperidou, C., Kug, J.-S., et al. (2021). Changing El Niño–Southern Oscillation in a warming climate. *Nature Reviews Earth & Environment*, *2*(9), 628–644. https://doi.org/10.1038/s43017-021-00199-z

Capotondi, A., Wittenberg, A. T., Kug, J.-S., Takahashi, K., & McPhaden, M. J. (2020). ENSO diversity. In M. J. McPhaden, A. Santoso, & W. Cai (Eds.), *El Niño southern oscillation in a changing climate*. https://doi.org/10.1002/9781119548164.ch4

Capotondi, A., Wittenberg, A. T., Newman, M., Di Lorenzo, E., Yu, J. Y., Braconnot, P., et al. (2015). Understanding ENSO diversity. *Bulletin of the American Meteorological Society*, *96*, 921–938. https://doi.org/10.1175/BAMS-D-13-00117.1

Coffel, E. D., Horton, R. M., & De Sherbinin, A. (2018). Temperature and humidity based projections of a rapid rise in global heat stress exposure during the 21st century. *Environmental Research Letters*, *13*(1), 014001. https://doi.org/10.1088/1748-9326/aaa00e

Davies-Jones, R. (2008). An efficient and accurate method for computing the wet-bulb temperature along pseudoadiabats. *Monthly Weather Review*, *136*(7), 2764–2785. https://doi.org/10.1175/2007MWR2224.1

Foster, J., Smallcombe, J. W., Hodder, S., Jay, O., Flouris, A. D., Nybo, L., & Havenith, G. (2021). An advanced empirical model for quantifying the impact of heat and climate change on human physical work capacity. *International Journal of Biometeorology*, *65*(7), 1215–1229. https://doi.org/10.1007/s00484-021-02105-0

Freychet, N., Hegerl, G. C., Lord, N. S., Lo, Y. T. E., Mitchell, D., & Collins, M. (2022). Robust increase in population exposure to heat stress with increasing global warming. *Environmental Research Letters*, *17*(6), 064049. https://doi.org/10.1088/1748-9326/ac71b9

Hersbach, H., Bell, B., Berrisford, P., Biavati, G., Horányi, A., Muñoz Sabater, J., et al. (2023). ERA5 hourly data on pressure levels from 1940 to present [Dataset]. *Copernicus Climate Change Service (C3S) Climate Data Store (CDS)*. https://doi.org/10.24381/cds.bd0915c6

Im, E.-S., Pal, J. S., & Eltahir, E. A. B. (2017). Deadly heat waves projected in the densely populated agricultural regions of South Asia. *Science Advances*, *3*(8), e1603322. https://doi.org/10.1126/sciadv.1603322

Jia, L., Delworth, T. L., Yang, X., Cooke, W., Johnson, N., Zhang, L., et al. (2024). Seasonal predictions of summer compound humid heat extremes in the southeastern United States driven by sea surface temperatures. *NPJ Climate and Atmospheric Science*, *7*(1), 180. https://doi.org/10.1038/s41612-024-00723-0

Jones, B., & O'Neill, B. C. (2016). Spatially explicit global population scenarios consistent with the shared socioeconomic pathways. *Environmental Research Letters*, *11*(2016), 084003. https://doi.org/10.1088/1748-9326/11/8/084003

Jones, B., & O'Neill, B. C. (2020). Global one-eighth degree population base year and projection grids based on the shared socioeconomic pathways, revision 01. Version 1.01 [Dataset]. *Archived by National Aeronautics and Space Administration, U.S. Government, NASA Socioeconomic Data and Applications Center (SEDAC)*. https://doi.org/10.7927/m30p-j498

Karamperidou, C. (2024). Extracting paleoweather from paleoclimate through a deep learning reconstruction of Last Millennium atmospheric blocking. *Communications Earth & Environment*, *5*(1), 535. https://doi.org/10.1038/s43247-024-01687-y

Karamperidou, C., & DiNezio, P. N. (2022). Holocene hydroclimatic variability in the tropical Pacific explained by changing ENSO diversity. *Nature Communications*, *13*(1), 7244. https://doi.org/10.1038/s41467-022-34880-8

Karamperidou, C., Jin, F. F., & Conroy, J. L. (2017). The importance of ENSO nonlinearities in tropical Pacific response to external forcing. *Climate Dynamics*, *49*(7–8), 2695–2704. https://doi.org/10.1007/s00382-016-3475-y

Kong, Q., & Huber, M. (2024). A global high-resolution and bias-corrected dataset of CMIP6 projected heat stress metrics [Dataset]. *Zenodo*. https://doi.org/10.5281/zenodo.13821299

Liu, C., An, S. I., Jin, F. F., Stuecker, M. F., Zhang, W., Kug, J.-S., et al. (2023). ENSO skewness hysteresis and associated changes in strong El Niño under a CO_2 removal scenario. *NPJ Climate and Atmospheric Science*, *6*(1), 117. https://doi.org/10.1038/s41612-023-00448-6

Lu, B., Chu, P., Kim, S., & Karamperidou, C. (2020). Hawaiian regional climate variability during two types of El Niño. *Journal of Climate*, *33*(22), 9929–9943. https://doi.org/10.1175/JCLI-D-19-0985.1

Matthews, T. (2018). Humid heat and climate change. *Progress in Physical Geography: Earth and Environment*, *42*(3), 391–405. https://doi.org/10.1177/0309133318776490

McKenna, M., & Karamperidou, C. (2023). The impacts of El Niño diversity on Northern Hemisphere atmospheric blocking. *Geophysical Research Letters*, *50*(13), e2023GL104284. https://doi.org/10.1029/2023GL104284

Menzo, Z., Karamperidou, C., Kong, Q., & Huber, M. (2024). El Niño enhances exposure to humid heat extremes with regionally varying impacts during eastern vs central Pacific events [Dataset]. *Zenodo*. https://doi.org/10.5281/zenodo.11392152

Raymond, C., Matthews, T., & Horton, R. M. (2020). The emergence of heat and humidity too severe for human tolerance. *Science Advances*, *6*(19), eaaw1838. https://doi.org/10.1126/sciadv.aaw1838

Rivera Tello, G. A., Takahashi, K., & Karamperidou, C. (2023). Explained predictions of strong eastern Pacific El Niño events using deep learning. *Scientific Reports*, *13*(1), 21150. https://doi.org/10.1038/s41598-023-45739-3

Rogers, C. D. W., Ting, M., Li, C., Kornhuber, K., Coffel, E. D., Horton, R. M., et al. (2021). Recent increases in exposure to extreme humid-heat events disproportionately affect populated regions. *Geophysical Research Letters*, *48*(19), e2021GL094183. https://doi.org/10.1029/2021GL094183

Schär, C. (2016). The worst heat waves to come. *Nature Climate Change*, *6*(2), 128–129. https://doi.org/10.1038/nclimate2864

Seneviratne, S. I., Donat, M. G., Pitman, A. J., Knutti, R., & Wilby, R. L. (2016). Allowable CO_2 emissions based on regional and impact-related climate targets. *Nature*, *529*(7587), 477–483. https://doi.org/10.1038/nature16542

Seneviratne, S. I., & Hauser, M. (2020). Regional climate sensitivity of climate extremes in CMIP6 versus CMIP5 multimodel ensembles. *Earth's Future*, *8*(9). https://doi.org/10.1029/2019ef001474

Sherwood, S. C., & Huber, M. (2010). An adaptability limit to climate change due to heat stress. *Proceedings of the National Academy of Sciences of the United States of America*, *107*(21), 9552–9555. https://doi.org/10.1073/pnas.0913352107

Simpson, C. H., Brousse, O., Ebi, K. L., & Heaviside, C. (2023). Commonly used indices disagree about the effect of moisture on heat stress. *NPJ Climate and Atmospheric Science*, *6*(1), 78. https://doi.org/10.1038/s41612-023-00408-0

Simpson, C. H., Brousse, O., Heaviside, C., & Ebi, K. (2023). Commonly used indices disagree about the relative effect of moisture on heat stress—Code supplement (v0.3) [Dataset]. *Zenodo*. https://doi.org/10.5281/zenodo.8038787

Song, F., Zhang, G. J., Ramanathan, V., & Leung, L. R. (2022). Trends in surface equivalent potential temperature: A more comprehensive metric for global warming and weather extremes. *Proceedings of the National Academy of Sciences of the United States of America*, *119*(6), e2117832119. https://doi.org/10.1073/pnas.2117832119

Speizer, S., Raymond, C., Ivanovich, C., & Horton, R. M. (2022). Concentrated and intensifying humid heat extremes in the IPCC AR6 regions. *Geophysical Research Letters*, *49*(5), e2021GL097261. https://doi.org/10.1029/2021GL097261

Takahashi, K., Montecinos, A., Goubanova, K., & Dewitte, B. (2011). ENSO regimes: Reinterpreting the canonical and Modoki El Niño. *Geophysical Research Letters*, *38*(10), L10704. https://doi.org/10.1029/2011GL047364

Taschetto, A. S., Rodrigues, R. R., Meehl, G. A., McGregor, S., & England, M. H. (2016). How sensitive are the Pacific–tropical North Atlantic teleconnections to the position and intensity of El Niño-related warming? *Climate Dynamics*, *46*(5–6), 1841–1860. https://doi.org/10.1007/s00382-015-2679-x

Vanos, J., Guzman-Echavarria, G., Baldwin, J. W., Bongers, C., Ebi, K. L., & Jay, O. (2023). A physiological approach for assessing human survivability and liveability to heat in a changing climate. *Nature Communications*, *14*(1), 7653. https://doi.org/10.1038/s41467-023-43121-5

Vecellio, D. J., Huber, M., & Kenney, W. L. (2024). Why not 35°C? Reasons for reductions in limits of human thermal tolerance and their implications. *Temperature*, *11*(4), 302–304. https://doi.org/10.1080/23328940.2024.2399952

Vecellio, D. J., Kong, Q., Kenney, W. L., & Huber, M. (2023). Greatly enhanced risk to humans as a consequence of empirically determined lower moist heat stress tolerance. *Proceedings of the National Academy of Sciences of the United States of America*, *120*(42), e2305427120. https://doi.org/10.1073/pnas.2305427120

Vecellio, D. J., Wolf, S. T., Cottle, R. M., & Kenney, W. L. (2022). Evaluating the 35°C wet-bulb temperature adaptability threshold for young, healthy subjects (PSU HEAT Project). *Journal of Applied Physiology*, *132*(2), 340–345. https://doi.org/10.1152/japplphysiol.00738.2021

Wyman, D. A., Conroy, J. L., & Karamperidou, C. (2020). The tropical Pacific ENSO–mean state relationship in climate models over the Last Millennium. *Journal of Climate*, *33*(17), 7539–7551. https://doi.org/10.1175/JCLI-D-19-0673.1